

Utilization of Agro-Waste Material RHA in to a Mesoporous Material SBA-16

S.B.Shete

Department of Electronics, S.G.B. College, Purna (Jn) – 431 511.

Email:s.bshete@rediffmail.com

Abstract: Spherical particles of mesoporous silica SBA-16 with cubic Im3m structure were synthesized at low pH using Pluronic F127 as template and RHA as silica source. The diameter of the spherical particles can be controlled in the range of 0.5–8 μm by varying Spherical particles of mesoporous silica SBA-16 with cubic Im3m structure were synthesized at low pH using Pluronic F127 as template and RHA as silica source. It is suggested that this morphology transition is due to a change in hydrolysis and condensation rate of the silica source and as a result the assembly of F127 micelles will differ. The SBA-16 samples were characterized using powder X-ray diffraction (XRD), scanning electron microscopy (SEM), transmission electron microscopy (TEM) and Nitrogen adsorption techniques.

Keywords: SBA-16; Spherical particles; Synthesis temperature; Morphology; Pluronic F127

Introduction:

Spherical particles of mesoporous silica SBA-16 with cubic Im3m structure were synthesized at low pH using Pluronic F127 as template and RHA as silica source. The diameter of the spherical particles can be controlled in the range of 0.5–8 μm by varying .The synthesis of mesoporous materials by a liquid-crystal template mechanism was reported (Beck J.S., *et al* 1992, Kresge C.T., *et al* 1992). The properties of these materials make them attractive for adsorption, catalysis, separation, chemical sensing, optical coating, drug delivery and electronic applications. For practical purposes, the overall morphology of a mesoporous material is a necessary requirement in combination with their internal structure. SBA-16 is a mesoporous material with 3D cubic pore arrangement corresponding to Im3m space group (Boissiere C., *et al* 2001). In this body-centred-cubic structure each mesoporous is connected with its eight nearest neighbours to form a multidirectional system of mesoporous network (Sakamoto Y, *et al* ,2000), Due to its large cage, high surface area and high thermal stability. (Hudson SP., *et al* 2008), this material appears to be one of the best candidates for catalytic support and packing materials for separation. Using F127 as a surfactant is the common way of synthesizing SBA-16(Zhao D., *et al* 1998, Van der Voort P. *et al* 2002). However, there are also reports on alternative surfactants such as F108 (Kipkemboi P., *et al* 2001), a blend of P123 and F127 . Micro porous zeolite are widely used as solid acid catalysts, (Shaodian Shen, *et al* 2007)but their applications are intrinsically limited by drawback of zeolite is that the small size of the channels (less than 0.8 nm) and cavities (<1.5 nm) imposes diffusion limitations on reactions that can cause high back pressure on flow systems. The dimensions of the zeolite micro pores (< 2 nm), mesoporous (2-50nm) and macro pores (> 50 nm) permit faster migration of guest molecules in the host frameworks. Since fast mass transfer of the reactants and products to and from the active sites is required for catalysts (Kresge C.T., *et al* 1992), the concept of infusing mesoporous into zeolite particles has attracted much attention. Recent progress involving this issued to ordered mesoporous materials such as MCM-41, SBA-16 and SBA-15. These mesoporous materials have pore diameters of 3.0 nm–8.0nm and exhibit catalytic properties for the catalytic conversion of bulky reactants, but unfortunately, when compared with micro porous zeolite (Kecht J., *et al*, 2008), the catalytic activity and hydrothermal stability are relatively low, which can be attributed to the amorphous nature of the mesoporous walls. To overcome this problem, some recent research efforts have been concentrated on introducing mesoporous or macro pores linked to the zeolite micro pores. These materials called Hierarchical zeolite materials with combinations of micro/meso/macro pores would further extend the application of zeolite as solid acid (Van der Voort P., *et al* 2002) .

Material and methods: SBA composite with different concentrations have been prepared under acidic conditions in the presence of triblock copolymer F127 by using RHA as silica source 1.6gm of F127 was dissolved in 120gm of H₂O, 5gm of conc. HCL and 7.5gm of butanol under magnetic stirring 1h to obtain homogeneous solution at 45⁰C to this solution 4.5gm of RHA was added. The mixture was stirred for another 24 hours. Ultrasonic treatment is given at power 70 for 30 min Then the solution is taken Teflon coated autoclave and hydrothermal treatment is given to 80⁰C for 24 hrs The synthesized mesoporous composite was filtered and dried in air. The sample is calcined at 1.5⁰C/min. at 550⁰C for 6h (Carniato Fabio *et al* 2012).

Result and discussion:

XRD-studies:

As-synthesized forms of RHA-SBA-16 (60, 70, 80 and 90) exhibit a typical pattern with a very strong (110) reflection at low angle 1.14⁰ and other weaker reflections as shown in Fig.1 A-(70, 80). According to Beck *et.al* these reflection lines can be indexed based on a hexagonal unit cell parameter ($a_0 = \sqrt{2}d_{110}$). In the XRD pattern of the calcined RHA-SBA-16(60⁰C), only the (110) reflection is observed prominently. The presence of only (110) reflection in the calcined sample suggests that this material does not possess the well defined hexagonal arrays after calcinations.

In both the as-synthesized and calcined samples, the mainly strong peak with (110) reflection is swung to higher d_{110} spacing values with increase in temperature of hydrothermal synthesis from 60⁰C to 90⁰C and afterwards it lowers (Fig.1A) and (Fig.1 B).

The sample RHA-SBA-16(80) in its as-synthesized form shows a different XRD pattern as in Fig. 1-A. The higher angle peaks due to (110) and other reflections are likely to fuse together forming one broad peak. This is due to the instability of the sample at the higher temperature, required for the removal of surfactant molecules present between the silicate sheets.

% Crystallinity and Activation Energy:

The percent crystallinity of the samples drawn at different synthesis temperatures in the crystallization kinetic was obtained by the following relation.

$$\% \text{ Crystallinity} = \frac{\text{Sum of the peak heights of unknown material} \times 100}{\text{Sum of peak heights of standard material}}$$

The characteristic peaks of RHA-SBA-16 starts appearing after 75⁰C and the fully crystalline phase is obtained around 80⁰C (with $2\theta \cong 1.14^0, 2.53^0, 3.24^0$ and 5.20^0 values). This unusual shorter crystallization temperature may be due to higher reactivity of the source of silica extract derived from RHA. The most crystalline sample in the synthesis system was treated as 100 % crystalline. It is also observed from the powder XRD profiles that obtained characteristic peaks closely match with the reported data.

Table 1 summarizes the values of inter planar spacing (d values) derived from X-ray diffraction pattern for RHA-SBA-16 (100 % crystalline) and was used as a parent sample for further study. The kinetic curve describing the increase in the crystallinity of the crystals with the synthesis temperature (before and after calcination) is nearly "S" shaped that depends on rate of conversion. This type of sigmoidal nature of crystallization curve indicates two distinct stages, namely an induction period and a crystal growth period. It is seen from the Fig. 1 (C) that up to 60⁰C the rate of conversion of amorphous to crystallization of RHA-SBA-16 phase was initially slow and then it increased sharply between 70⁰C to 80⁰C followed by subsequent slow down. By the application of Arrhenius equation to the kinetics of crystallization of RHA-SBA-16, apparent activation energy of conversion of aluminosilicate gel to 100% crystalline phase was found to be 106.12 kJmole⁻¹ in the present crystallization system.

BET surface area and pore volume of RHA-SBA-16

The samples synthesized at different temperatures have also been characterized by N₂-adsorption-desorption study. The isotherms obtained from N₂-adsorption-desorption and corresponding BJH pore size distribution is shown in Fig. 2 (A, B). According to IUPAC classification, these isotherms of RHA-SBA-16 are of type IV, which is the characteristic of mesoporous material. The isotherms exhibit three stages. The first stage is a linear part almost going through the origin, which is due to monolayer adsorption of nitrogen on the walls of the mesoporous ($p/p_0 < 0.2$). The second stage is characterized by a steep increase in adsorption (within the relative pressure p/p_0 range of 0.2-0.4) due to capillary condensation of N₂ in the pore channels. This part shows hysteresis.

The p/p_0 value at which the inflection starts is related to the diameter of the mesoporous. The sharpness in this step indicates the uniformity of the pore size distribution. The third stage in the adsorption isotherm is an almost horizontal part after the relative pressure p/p_0 of ~0.35 and is due to multilayer adsorption on the outer surface of the particles. In addition, a hysteresis loop at relative pressure $p/p_0 > 0.8$ corresponds to a capillary condensation in the inter particle pores.

For Samples RHA-SBA-16 (60) and RHA-SBA-16 (80), a linear increase in adsorption at low pressures is observed followed by a steep increase in nitrogen uptake [at a relative pressure of $p/p_0 = 0.31-0.41$ and $0.25-0.35$ for RHA-SBA-16(60) and RHA-SBA-16(80), respectively due to capillary condensation inside the mesoporous Fig. 2 (A) for RHA-SBA-16(60, 70, 80). The broad hysteresis loop in the isotherm for RHA-SBA-16(60) reflects disorder in the shape and size of the mesoporous. This step of the isotherm is sharper for RHA-SBA-16(80) indicating a narrow pore size distribution. Thus, as the crystallization temperature increases from 60^oC to 80^oC, the step of the isotherm becomes sharper indicating narrower pore size distribution Fig. 2 (B) for RHA-SBA-16 (60, 70, and 80)

The N₂-adsorption-desorption isotherms and the pore size distribution of the Sample RHA-SBA-16 (90) are found that the hysteresis loop is a wide range of relative pressures, p/p_0 (0.28-1.00). The shape of the hysteresis loop confirms the formation of a lamellar phase. The pore size distribution becomes broader.

Thus, the XRD results are confirmed by N₂-adsorption-desorption data, which are similar to those, reported for SBA-16. In pore size distribution curve, narrow and sharp peak is observed in the diameter range 20-25 Å showing uniform pore size. The isotherms of the RHA-SBA-16 samples show small hysteresis loop in the lower pressure regions. We noted that the surface areas of calcined RHA-SBA-16 samples are comparatively more than as synthesized RHA-SBA-16 and it is increasing with the increase in crystallization temperature. The more surface area (788.6 m²/g) is an indication of well narrow dispersion of pores.

Table 1 presents a summary of all the parameters obtained by nitrogen sorption and powder X-ray diffraction pattern. The unit cell parameter (a_0) has been calculated by the formula $a_0 = \sqrt{2} d_{110}$. The wall thickness has been calculated by subtracting the pore diameter obtained from N₂-sorption from the unit cell parameter (a_0). It is observed from the tabulated data that spacing value of most intense peak at d_{110} is slightly increase and the pore diameter is decreased with increase in temperature of hydrothermal synthesis from 60^oC to 80^oC. It is due to increase in the wall thickness of the pores of RHA-SBA-16. The surface area is increased with the increase in synthesis temperature from 60^oC to 90^oC due to the progressive formation of ordered mesophase silica. However, the surface area decreases with further increase in synthesis temperature due to silica pore shrinkage. This suggests that increasing the synthesis temperature can accelerate the silicate condensation on the silica wall, which subsequently thickens the silica framework.

Thus, the above results indicate that in hydrothermal synthesis of RHA-SBA-16 molecular sieves, temperature plays a significant role. An increase of the crystallization temperature from 60^oC to 80^oC increases the long-range order in the structure as well as the wall thickness of the RHA-SBA-

16 molecular sieves. However, with further increase in the temperature to 90⁰C, the hexagonal phase changes to a lamellar one under the synthesis conditions.

FTIR-studies:

The FTIR spectra of RHA-SBA-16 (60, 70, and 80) after calcination are illustrated in Fig.3. The broad band around 3450 cm⁻¹ is due to surface silanols and adsorbed water molecules which indicate the silica framework is hydrophilic. For calcined RHA-SBA-16, the disappearance of peak at 2879.2 cm⁻¹ and 2842.3 cm⁻¹ can be concluded that the calcination at 550⁰C is complete. This indicates that the organic template has been removed completely due to calcination. RHA-SBA-16 tends to adsorb water vapors in air since the surface of silica framework is water liking, the stretching mode of H₂O is observed at 1585.6cm⁻¹. Bands observed at 1154.7 cm⁻¹ and 1084.0 cm⁻¹ are characteristics peaks of asymmetric Si-O-Si stretching. Another characteristics peak is the symmetric Si-O-Si stretching observed at 795.6 cm⁻¹. However, the peak at 2325.2 cm⁻¹ is prominently found to be changed due to the effect of synthesis temperature. The effect observed for RHA-SBA-16(80) is noticeable, which is also supported by the XRD analysis and sorption studies of the samples.

V) SEM and TEM-Analysis:

SEM images of RHA-SBA-16(60, 80) are depicted in Fig.4 represents that the ensuing particles are roughly spherical in shape with no agglomerations. Small spherical particles are of RHA-SBA-16(80) with diameters of 7.6 to 18.4A⁰.

It is observed that the average diameter of the particles is slightly increased as the synthesis temperature is elevated from 60⁰C to 90⁰C after calcination. However when the synthesis temperature was around 80⁰C, the prepared sample has signified a high-quality structural morphology.

TEM-Analysis:

Fig. 5 represents the TEM images of RHA-SBA-16 synthesized at 80⁰C. TEM image of the parent RHA-SBA-16 samples provided strong confirmation of the retainment of mesoporous structure of the supports. The characteristic hexagonal silicate structures shown on TEM, supports the observation made by low angle XRD.

Table 1: Effect of crystallization temperature on Structural and textural properties of RHA-SBA-16

As synthesized Samples	d ₁₁₀	Unit cell parameter	S.A. (m ² /g)	Average pore diameter(Å)	Pore volume (ml/g)	Average wall thickness (Å)	% Crystallinity
RHA-SBA-16(60)	20.13	28.99	217.22	--	-	--	10
RHA-SBA-16(70)	21.51	30.97	326.42	--	-	--	22
RHA-SBA-16(80)	23.44	33.75	701.35	25.32	0.416	8.43	71
RHA-SBA-16(90)	23.12	33.29	606.70	24.91	0.488	8.38	67
For Calcined Samples							
RHA-SBA-16(60)	23.43	33.74	664.34	25.63	0.492	8.11	41
RHA-SBA-16(70)	25.55	36.79	711.65	27.33	0.523	9.46	60
RHA-SBA-16(80)	26.93	38.78	779.70	29.16	0.568	9.62	100
RHA-SBA-16(90)	23.68	34.10	689.21	25.21	0.501	8.89	87

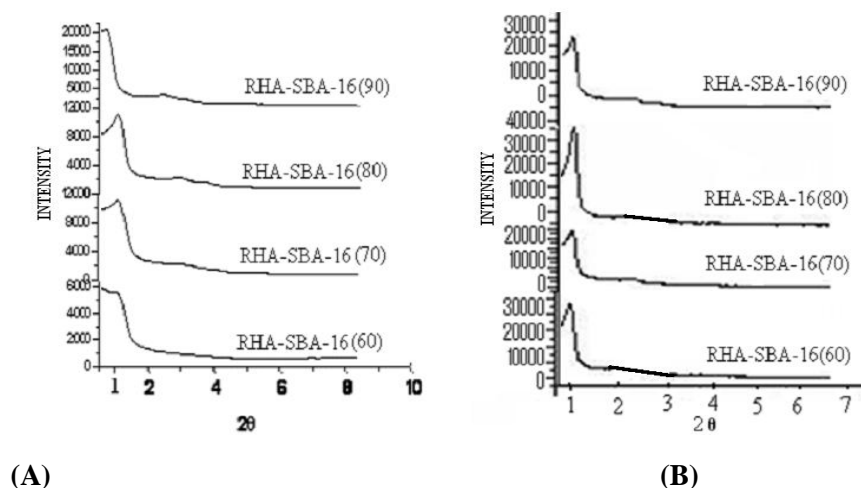


Fig. 1: XRD patterns of (A) as-synthesized and (B) calcined samples of RHA-SBA-16(60°C to 90°C) for synthesis temperatures 60°-90°C

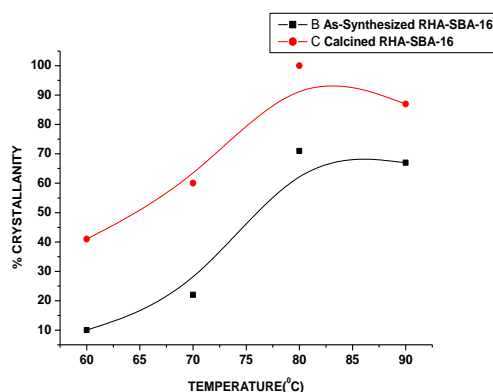


Fig.1: (C) Effect of synthesis temperature on crystallization

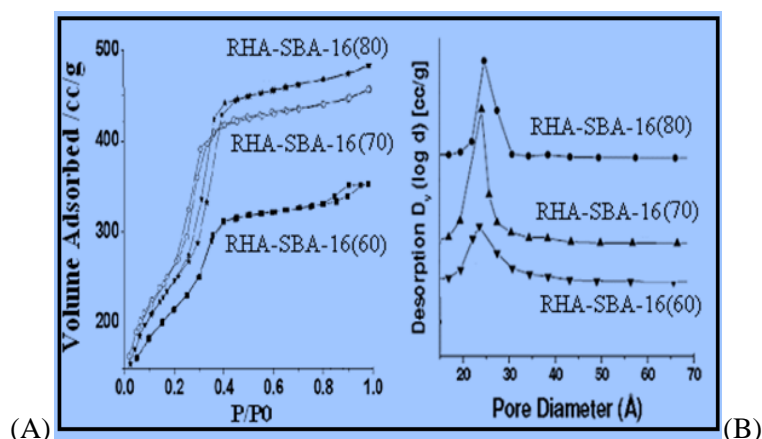


Fig.2: (A) N₂ adsorption-desorption isotherms and (B) pore size distribution of RHA-SBA-16 (60, 70, 80) synthesized at 60°-80°C

Highest surface area was found for the sample with pH of 6.9. It is also revealed from the data, that as the pH value increases, surface area also increases but when it declines to more acidity or basicity it gets drastically reduced from with subsidiary change in the average

pore diameter and wall thickness. This is because at high pH, solubility of silica increases rapidly due to which a higher amount of silica is left in the solution at the end of the synthesis. As the pH increases up to 6.9 the nucleation rate becomes higher forming smaller particles and higher surface area as statistically expressed in table 1.

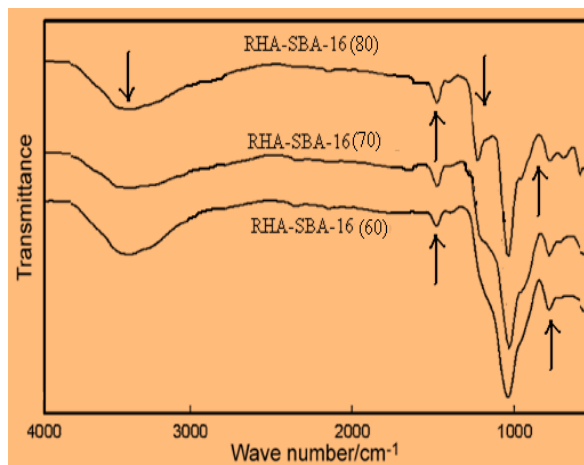


Fig. 3: FTIR spectrum of RHA-SBA-16 (60, 70, 80) Synthesized at 60, 70 and 80°C

are illustrated in Fig.3. The broad band around 3500.2 cm^{-1} indicates hydrophilicity of silica framework. The appearance of peaks at 2932.1 cm^{-1} and 2843.8 cm^{-1} for samples can be concluded due to the effect of Sulphate ions of H_2SO_4 during precipitation. However, the peak at 2932.1 cm^{-1} is prominently found to be changed due to the effect of pH during synthesis.

The effect observed for RHA-SBA-16 (6.9) is significant, which is well supported by the XRD analysis and sorption studies of the samples. Rest of the peaks represents the usual stretching for functional groups involved in SBA-16.

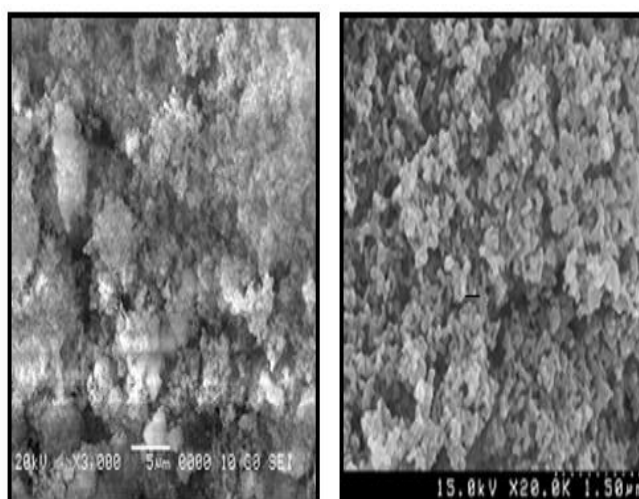


Fig. 4: SEM images of RHA-SBA-16(60, 80) synthesized at 60 and 80°C

The morphology of the RHA-SBA-16 as a function of pH of gel was directly monitored by SEM as shown in Fig.4.

The SEM results indicate that the material surface starts to become rough and form nano-scale particles above pH 6.9 the nano-scale particles increases with further increasing pH. SEM images of RHA-SBA-16 (6.9, 7.8) are depicted in Fig.4 represents that the resulting

particles are almost spherical in shape having diameters ranging from 2.0-14.0A⁰ without agglomerations.

It is observed that the average diameter of the particles is considerably altered as the pH is raised from 2.3 to 8.6. However when the pH of gel was around 6.9, the prepared sample indicated a good structural morphology.

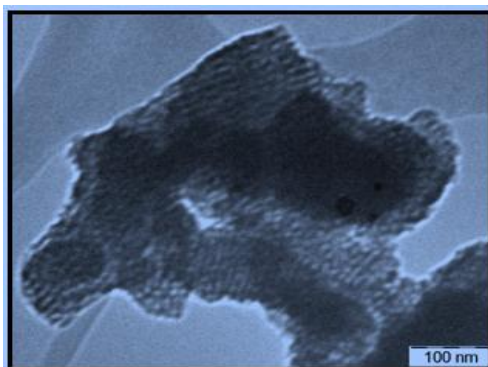


Fig. 5: TEM images of RHA-SBA-16(80) synthesized at 80°C

Fig.5. represents the TEM images of RHA-SBA-16 synthesized at 80°C and calcined at 550°C. TEM image of the parent RHA-SBA-16 samples provided sturdy verification of the retainment of mesoporous structure. The characteristic hexagonal silicate structures shown on TEM, supports the observation made by low angle XRD.

CONCLUSION:

The correlation of the work reported by (Carniato Fabio *et al* 2012) is using commercially available chemicals but our research is by using low cost waste material. We got the same result as reported.

All the characterization techniques performed in this study reveals that well ordered mesoporous material of uniform hexagonal array can be synthesized very conveniently and in a very short span of time from an agro waste rice husk ash instead of commercial expensive silica sources. The parametric variation such as change of synthesis temperature helps to optimize the synthesis conditions. The well ordered mesoporous material RHA-SBA-16 can be synthesized at 80°C for 4.5h keeping pH of gel 6.9 and calcined at 550°C. The apparent activation energy of conversion of synthesis gel to 100 % crystalline RHA-SBA-16 phase was 184.62kJ/mole calculated by Arrhenius equation.

References:

1. Beck J.S., Vartuli J.C., Roth W.J., Leonowicz M.E., Kresge C.T., Schmitt K.D., W Chu C.T., D.H. Olson, E.W. Sheppard, S.B. McCullen, J.B. Higgins, J.L. Schlenker, (1992). A New Family of Mesoporous Molecular Sieves Prepared with Liquid Crystal Templates *J. Am. Chem. Soc.*;114:10834–43.
2. Boissiere C., Kummel M., Persin M., Larbot A. and Prouzet E., *Adv. Funct. Mater* (2001). Porosity and Mechanical Properties of Mesoporous Thin Films Assessed by Environmental Ellipsometric Porosimetry. 129
3. Carniato Fabio, Paul Geo, Stefano Chiara Bisio Caldarelli and Marchese Leonardo (2012), On the organic/inorganic interface between mesoporous SBA-16 silica and its structural directing polymer: a combined FT-IR and solid state NMR study 1153–1160
4. Hudson SP, Padera RF, Langer R, Kohane DS. (2008) The biocompatibility of mesoporous silicates. *Biomaterials*. 29:4045–55.
5. Kecht J, Schlossbauer A, Bein T. (2008) Selective functionalization of the outer and inner surfaces in mesoporous silica nanoparticles. *Chem Mater*.;20:7207–14.

6. Kipkemboi P., Fogden A., Alfredsson V., Flodström K., Langmuir 17 (2001) Triblock Copolymer as Templates in Mesoporous Silica Formation: Structural Dependence on Polymer Chain Length and Synthesis Temperature 5398.
7. Kresge C.T., Leonowicz M.E., Roth W.J., Vartuli J.C., Beck J.S., (1992) Nature 359
Ordered mesoporous molecular sieves synthesized by a liquid-crystal template mechanism 710.
8. Sakamoto Y., Kaneda M., Terasaki O., Zhao D.Y., Kim J.M., Stucky G., Shin H.J., Ryoo R., Nature 408 (2000) 449.
9. Shaodian Shen, Deng Yan, Zhu Guibo, Dongsen Mao; Wang Yuhong, Guishen Wu, Jun Li, Xiao Zhen Liu, Guanzhong Lu, Zhao Dongyuan. (2007) J Mater Sci. A Zeolite-Like Zinc Phosphonocarboxylate Framework and Its Transformation into Two- and Three- Dimensional Structures 7057–7061
10. Van der Voort P., Benjelloun M., Vansant E.F, (2002) Rationalization of the synthesis of SBA- 16: controlling the micro- and mesoporosity. J. Phys. Chem. B 106 9027.
11. Zhao D., Huo Q., Feng J., Chmelka B.F., Stucky G.D., (1998) J. Am. Chem. Soc. 120 Triblock-Copolymer-Directed Syntheses of Large-Pore Mesoporous Silica Fibers 6024.